

World In Your Hands: A Large-Scale and Open-Source Ecosystem for Learning Human-Centric Manipulation in the Wild

Yupeng Zheng*, Jichao Peng*, Weize Li*, Yuhang Zheng, Xiang Li, Yujie Jin, Julong Wei, Guanhua Zhang, Ruiling Zheng, Ming Cao, Songen Gu, Zhenhong Zou, Kaige Li, Ke Wu, Mingmin Yang, Jiahao Liu, Pengfei Li, Hengjie Si, Feiyu Zhu, Wang Fu, Likun Wang, Ruiwen Yao, Jieru Zhao, Yilun Chen, Wenchao Ding†

Project Page: <https://wiyh.tars-ai.com>

Code: <https://github.com/tars-robotics/World-In-Your-Hands>

TARS Robotics

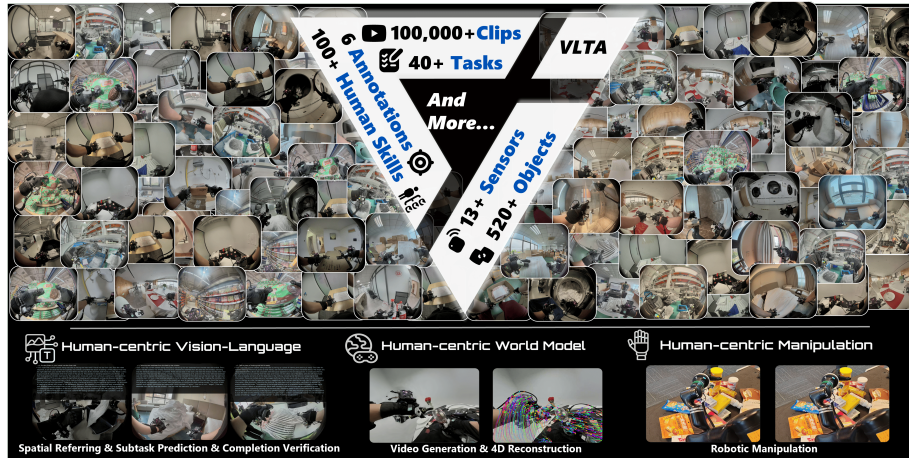


Fig. 1: Our World In Your Hands (WIYH) ecosystem is built on top of a large-scale self-collected dataset in real-world human environments. It captures human subjects performing over 40 distinct tasks across a wide variety of scenarios. The dataset provides rich RGB video streams, along with comprehensive motion ground truth encompassing more than 100 human skills. In addition to sensor and action data, it includes diverse annotations. This rich multimodal collection makes WIYH an excellent resource for research in spatial intelligence and embodied foundation model training.

Abstract. We introduce World In Your Hands (WIYH), a large-scale open-source ecosystem comprising over 1,000 hours of human manipulation data collected in-the-wild with millimeter-scale motion accuracy. Specifically, WIYH includes (1) the Oracle Suite, a wearable data collection kit with an auto-labeling

pipeline for accurate motion capture; (2) the WIYH Dataset, featuring over 1,000 hours of multimodal manipulation data across hundreds of skills in diverse real-world scenarios; and (3) extensive annotations and benchmarks supporting tasks from perception to action. Furthermore, experiments based on the WIYH ecosystem show that integrating WIYH’s human-centric data improves robotic manipulation success rates from 8% to 60% in cluttered scenes. World In Your Hands provides a foundation for advancing human-centric data collection and cross-embodiment policy learning. All data and hardware design will be open-source.

Keywords: Robotic Manipulation · Ego-centric Learning · System

1 Introduction

Large-scale pre-training has been established as a cornerstone for achieving generalization in Large Language Models [1, 8, 12, 44, 55], Vision-Language Models [2, 29–31, 38] and Vision-Language-Action (VLA) Models [6, 7, 26, 51, 56, 59]. However, datasets for dexterous hand manipulation remain far smaller and less diverse than language datasets, limiting progress in learning robust manipulation. To address the problem of data scarcity, human-centric data collection and learning have attracted growing interest [21, 24, 39, 57, 58]. Some approaches [5, 11, 28] capture human hand data during object manipulation using devices such as VR systems and smart glasses, while others [16, 18, 46, 53] leverage foundation models to extract human actions from unlabeled videos of human manipulation available on the internet.

Despite these advances, current human manipulation datasets still face three major limitations, as shown in Table 1 that hinder their usefulness for dexterous manipulation research: (1) **Limited Scenario Diversity:** Many datasets are collected in constrained laboratory environments, lacking the diversity and complexity of real-world settings. (2) **Inadequate Alignment:** Existing collections

Table 1: Comparison to existing datasets. WIYH is characterized by two key distinctions: (1) Its entire 1000 hours of data were collected in the wild, with the tasks performed by skilled practitioners, thereby capturing the most authentic decision-making processes and actions; (2) Despite the significant challenge of annotating such a diverse, real-world collection, WIYH provides comprehensive annotations, including motion ground truth, depth, masks, task/sub-task labels, and chain-of-thought (CoT) reasoning, etc.

Dataset	Hours	Clips	Wild	Cam. Calib	RGB	Tactile	Action	Depth	Mask	Instruct.	VLM
Ego4D [16]	3.670	✓	✓	✗	✓	✗	2D	✗	✗	✓	✓
HO4D [34]	44.4	4k	✓	✓	✓	✗	2D	✓	✓	✗	✗
HoloAssist [49]	166	2.22k	✗	✗	✓	✗	-	✓	✓	✓	✓
Ego-Exo4D [17]	1,286	5.04k	✓	✓	✓	✗	✗	✗	✓	✓	✓
CaptainCook4D [36]	94.5	384	✓	✗	✓	✗	✗	✓	✗	✓	✓
HOT3D [5]	13.9	425	✗	✓	✓	✗	3D	✗	✗	✗	✗
HO-Cap [45]	-	64	✗	✓	✓	✗	3D	✓	✓	✗	✗
Ego-ViD-5M [48]	-	5M	✗	✓	✓	✗	✗	✗	✓	✓	✗
EgoDex [20]	829	338k	✓	✗	✓	✗	3D	✗	✓	✓	✗
WIYH (Ours)	1045	125.4k	✓	✓	✓	✓	3D	✓	✓	✓	✓

often lack one or more key modalities, such as the absence of fine-grained language instructions, precise 3D action, or object poses, resulting in misalignment across vision, language, and action. (3) **Insufficient Benchmarking**: Most datasets do not support comprehensive evaluation benchmarks that span the entire pipeline of dexterous manipulation, including scene perception, task planning, and action.

To bridge this gap and investigate in-depth how human-centric data can advance dexterous manipulation, we introduce World In Your Hands (WIYH), a large-scale open-source ecosystem for learning human-centric manipulation in the wild, as shown in Figure 1. Specifically, the WIYH ecosystem comprises three core components:

- **The Oracle Suite**. We introduce a lightweight, flexible wearable data-collection kit that captures 3D action data with millimeter-scale translational accuracy (mean error below 5 mm) without external third-person tracking.
- **The WIYH Dataset**. We present a large-scale multi-modal resource comprising over 1,000 hours of manipulation demonstrations across 100 skills, captured in 10 diverse scenarios. The dataset includes rich sensory streams: multi-view images, camera calibration parameters, hand poses, and wrist trajectories.
- **Diverse Annotations**. Building upon the WIYH dataset, we provide extensive annotations, including 400 hours of atomic action instructions and 100k instances of vision-language data, supporting a comprehensive usage from scene perception to robotic manipulation.

Based on the WIYH ecosystem, we study how human-centric data empowers dexterous manipulation learning in robotic manipulation tasks. We conduct two sets of experiments: (1) cross-embodiment pretraining and (2) retargeting co-training, and evaluate the task success rate across varied environments and object layouts. Our experiments demonstrate that human-centric data substantially improves the generalization and robustness of robotic manipulation, whether as large-scale cross-embodiment pre-training data or retargeted action data.

Limitation. To increase accessibility and reproducibility, we are developing high-fidelity simulation environments and plan to release them in a future version of the dataset and benchmarks.

2 World In Your Hands Ecosystem

2.1 Oracle Suite: Human-centric Data Collection Suite

We develop **Oracle Suite**, a low-cost wearable data collection system designed for human-centric multimodal data collection. Specifically, as illustrated in Figure 2, Oracle Suite comprises a hardware system that captures multi-view RGB images, IMU-based localization, and tactile information and an autolabeling module that achieves high-precision motion capture by fusing IR, RGB, and IMU localization.



Fig. 2: Oracle Suite: Human-centric Data Collection Suite. It is primarily composed of three integrated components: (1) H-FPVHive: A first-person perception suite equipped with multiple cameras of different modalities to comprehensively record the operator’s environmental context. (2) H-Glove: A hand motion capture and tactile perception module. It integrates motion capture gloves, tactile sensors, and visual trackers. The H-Glove is synchronized with the H-FPVHive, enabling precise action localization and capture in unstructured, real-world settings. (3) H-Backpack: A power supply and data storage unit.

Hardware System Overview. Oracle Suite adopts a modular architecture integrating three primary hardware components: H-FPVHive, H-Gloves, and H-Backpack. This design enables flexible deployment across diverse environments without being restricted to stable indoor labs.

Hardware Design. The Oracle Suite incorporates significant optimizations in ergonomics, sensing, and reliability.

- **H-FPVHive** supports a chest-mounted configuration with two fisheye cameras, two pinhole cameras, and four infrared lenses integrated into the chest unit, where all cameras achieve hardware synchronization, and the infrared lenses facilitate better localization of the relative pose of H-Gloves.
- **H-Gloves** include six IMUs, five fingertip pressure sensors with a resolution of 5mN and a range of 0.2 N to 50 N, and an onboard MCU per glove to capture hand motions and tactile information while also containing three fisheye cameras for visual tracking and observation.
- **H-Backpack** provides data storage, computation, and power supply, utilizing an NVIDIA Orin computing core.

Autolabeling Pipeline. The autolabeling pipeline involves online and offline algorithms, as shown on the right side of Figure 2. By fusing multimodal sensor streams (IR, IMU, and RGB), it maintains robust localization in in-the-wild scenarios and ultimately outputs 6D wrist pose trajectories with millimeter-scale translational accuracy (mean positional error below 5 mm).

Efficiency of Oracle Suite. Compared to teleoperation, Oracle Suite achieves $5\times$ higher collection efficiency (720 vs. 150 episodes/day) without extensive operator training. Compared to VR-based hand tracking, Oracle Suite provides more accurate 3D hand skeletons, particularly under visual occlusion.

2.2 Data Validation System

We employ motion capture tests and projection intersection methods to validate data quality. Figure 3 illustrates the testing effects of both methods, and we retain valid high-quality data. For the motion capture test, we attach motion capture spheres to H-Gloves and complete operations identical to those in the WIYH dataset within a motion-capture room. This setup tests the deviation between the wrist trajectory generated by the Oracle Suite autolabeling pipeline and the motion capture trajectory to verify the effectiveness of the automatic annotation pipeline. Our Oracle Suite achieves an average position error of 5 mm in the motion capture room environment. For projection overlap, we obtain hand masks in perspective views of H-FPVHive using a hand segmentation algorithm. We then project the skeleton data from H-Gloves into the same view and calculate the intersection with the hand mask to determine accuracy.

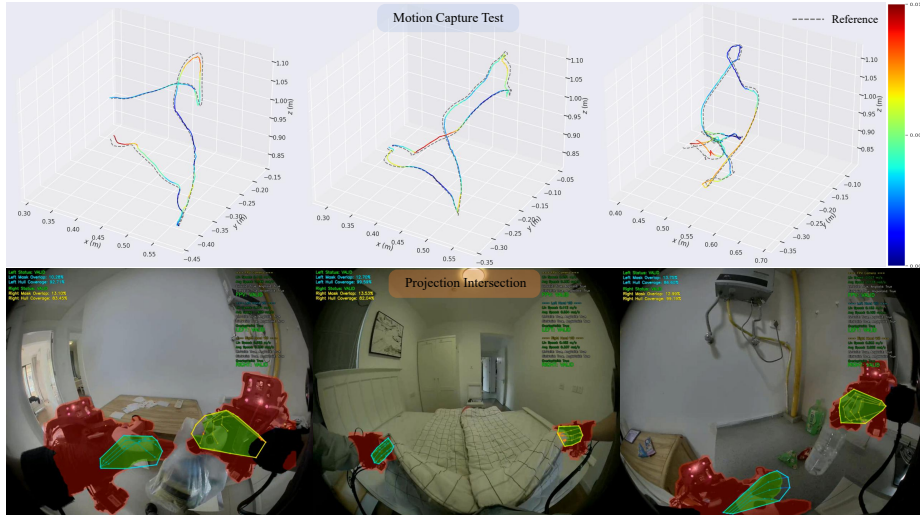


Fig. 3: WIYH Data Validation. The first row illustrates the motion capture test conducted in the mocap room. The dashed curve indicates the reference trajectory measured by the mocap system, while the solid curve denotes the trajectory estimated by the Oracle Suite. Color intensity encodes the deviation magnitude, with red indicating larger errors. In this controlled lab setting, the Oracle Suite achieves a mean translational error below 5 mm. The second row presents the projection-intersection check used to verify action accuracy. We compute an intersection score and flag samples whose score falls below a predefined threshold; these cases are then manually reviewed and filtered to ensure data quality.

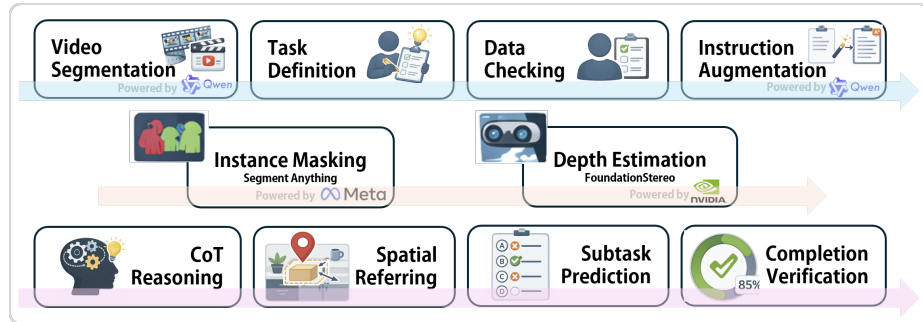


Fig. 4: Overview of WiYH dataset annotation pipeline. It consists of three stages: **atomic action annotation**, **perception annotation**, and **vision-language annotation**. Finally, all annotation information is manually reviewed by humans to ensure accuracy and consistency.

3 World In Your Hands Dataset

3.1 Data Collection and Annotation

Data collection: During data collection, collectors wear the Oracle Suite in various scenarios to record natural manipulation behaviors. Each task is recorded once according to the Standard Operating Procedure of the scenario. Recording sessions last approximately 10 minutes and include start and end event markers. Captured signals include tactile signals from pressure sensors, wrist images, first-person chest images, corresponding camera calibration parameters, left and right hand trajectory data, and left and right hand skeleton information. Samples of data annotations are shown in Figure 6.

After data collection, we curate the WIYH dataset via a three-stage annotation pipeline (Figure 4), comprising atomic action annotation, perception annotation, and vision-language annotation.

Atomic action annotation: To construct data suitable for robotic foundation model training, we design a four-stage hybrid annotation process for atomic action annotation that decomposes a task in the standard operating procedure into multiple atomic segments, where each segment is termed a subtask.

- **Video Segmentation:** The process initiates with video segmentation, where Qwen2.5-VL-72B [3] segments the recorded data for each task into semantic atomic fragments serving as basic units for annotation.
- **Task definition:** Humans define a preset action termed a "skill" and an operation target object for each atomic fragment.
- **Data checking:** Manual reviewers check boundary and task definition accuracy to correct errors.
- **Instruction Augmentation:** Post-processing combines the annotated preset actions and target object names into complete atomic instructions, which are augmented and enhanced using Qwen2.5-VL-72B [3].

Perception annotation: We use vision foundation models [27, 50] to pre-annotate scene elements, followed by manual selection and correction. This includes generating instance masks by applying SAM [27] to human-provided prompt points and estimating scene depth from first-person binocular images using the FoundationStereo [50] model.

Vision-language annotation is generated through manual curation and includes several components.

- **CoT Reasoning:** We use Qwen2.5-VL-72B [3] to generate a thought process indicating the position of each subtask within a complete task and when to enter the next subtask for long-horizon task decomposition, where generated thought data is reviewed and corrected by humans.
- **Spatial Referring (SR):** We select key frames near the action start where the operation target object is clearly visible for some subtasks and add spatial relation terms based on the atomic instruction to uniquely refer to a single target area in the scene.
- **Subtask Prediction (SP):** We select tasks containing 4 to 5 subtasks and use the next subtask after the current one as the correct option, while generating three logically reasonable incorrect options based on the task description.
- **Completion Verification (CV):** We randomly crop 0% to 35% of each subtask for a task and use the atomic instruction of each subtask, as well as the cropped fragment, as input to label the task progress status regarding whether the task is completed.

Notably, subtask prediction, spatial referring, and progress verification are annotated on only a subset of the whole WIYH data to construct an evaluation set for validating the capabilities of existing VLMs in human-centric scenarios.

3.2 Data Statistics

Figure 5 summarizes key statistics of our WIYH dataset. We first analyze the distribution of tasks across scenes. As shown in Figure 5(a), WIYH contains a diverse set of daily environments, including banquet, laundry, logistics, hotel, department, office, supermarket, industry, cleaning, and candlelight settings. The Sankey diagram illustrates the total accumulated duration of each task within its corresponding scene.

Scenes such as supermarkets and laundry include long-horizon activities with substantial execution time, while hotels and candlelight contain shorter but highly structured routines. This diversity in task-scene composition highlights the wide operational range covered by WIYH. Action-level temporal characteristics are shown in Figure 5(b). For each scene, we compute the average execution duration of fine-grained actions. The dataset exhibits substantial variation across action categories, from short, instantaneous operations such as "wipe" and "insert" to long-horizon manipulation such as "smooth out" or "fold lay". These temporal differences reflect the heterogeneous complexity of real-world household and industrial workflows.

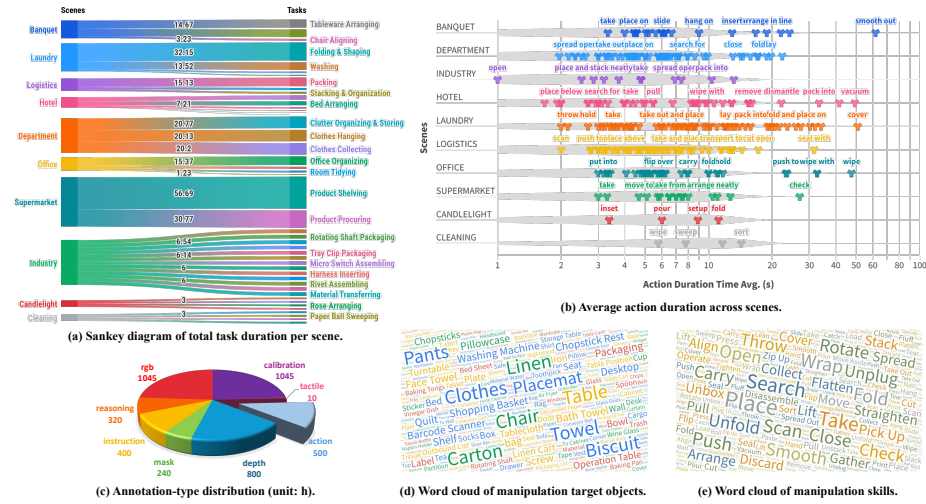


Fig. 5: Overview of dataset statistics, including task–scene relationships, action durations, annotation distributions, and word clouds of manipulation target objects and skills. The dataset spans a wide spectrum of real-world scenarios, from industrial to daily life (e.g., factories, hotels, apartments, supermarkets). For each scenario, it provides task and subtask annotations crucial for instruction–action alignment and task decomposition in robot learning. The chart presents multi-dimensional statistics of these annotations.

Figure 5(c) reports the distribution of annotation types. WIYH includes rich multimodal and task-level supervision, consisting of RGB, depth, action, instruction, reasoning, mask, tactile, and calibration annotations. Among them, RGB and calibration frames appear most frequently, while reasoning and tactile annotations, though smaller in quantity, provide high-level semantic cues crucial for complex manipulation and planning tasks.

To better understand the manipulation space in WIYH, Figure 5(d–e) visualizes word clouds of the annotated target objects and skills. The dataset covers a broad range of manipulable objects—including clothes, linens, cartons, cups, and tableware—spanning deformable, rigid, and articulated categories. Likewise, the skill vocabulary encompasses diverse manipulation primitives such as take, place, rotate, unfold, align, push, and search, representing both low-level motor actions and higher-level task strategies. These distributions further demonstrate that WIYH captures a wide spectrum of real-world manipulation behaviors. More data, demonstrations, and statistics will be provided in the supplementary materials.

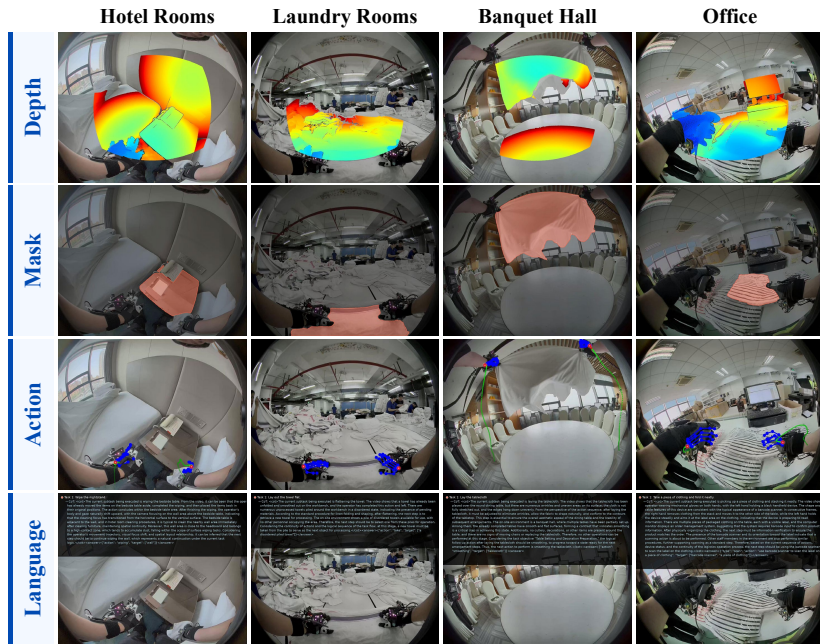


Fig. 6: Data annotation samples cross different scenes. The example of human-centric data annotations, including depth, mask, action, and task descriptions in four scenarios.

4 Benchmark and Application

4.1 Benchmark: Human-centric Vision-Language (HVL)

In this section, we construct three evaluation tasks based on the vision-language annotations introduced in Section 3. These tasks are designed to evaluate whether existing Multimodal Large Language Models (MLLMs) can achieve a genuine understanding of human-centric manipulation tasks in highly generalized, in-the-wild environments.

We define the following three evaluation tasks and test several closed-source and open-source MLLMs, including GPT-4o [23], Doubao-seed [4], and Qwen [55]. Detailed experimental setups and data statistics are provided in the supplementary material. (1) **Spatial Referring (S.R.)**: Given a human manipulation image and a description of the spatial relationships among multiple objects in the scene, the model is required to output the pixel coordinates of a specified region. Performance is measured by the probability that the predicted point lies within the target area. (2) **Subtask Prediction (S.P.)**: Given a piece of human manipulation video, the current task description, and four candidate options for the next action, the model must select the correct subsequent action. (3) **Completion Verification (C.V.)**: Given a piece of human manipulation video and the current task description, the model needs to determine whether

Table 2: Comparison of VLMs on spatial referring, subtask prediction, and completion verification tasks.

Model	S.R. (%)	S.P. (%)	C.V. (%)
GPT-4o [35]	10.04	73.40	51.18
Qwen3-VL-Plus [43]	46.53	71.75	55.89
Doubao-Seed-1.6-Vision [9]	39.83	76.84	51.96
Qwen3-VL-4B-Instruct [42]	25.58	69.21	56.73

the task has been completed. Evaluation details will be provided in the supplementary material. As shown in Table 2, scores for the S.R. task and C.V. task are generally low, whereas scores for the S.P. task remain relatively high. This discrepancy reflects the characteristics of existing VLMs, which demonstrate competent performance in high-level task decomposition but exhibit limitations in dynamic progress modeling and spatial understanding in specific embodied tasks. Specifically, on the S.R. task, scores of all VLMs are below 0.5, and on the C.V. task, all models perform slightly above 0.5, suggesting that their abilities in such contexts remain limited. Notably, Qwen3-VL-Plus, which was pre-trained on spatial-understanding data, achieves the best performance on the S.R. task. These experimental results collectively demonstrate that general-purpose, vanilla VLMs still fall short in embodied tasks. Our WIYH dataset, with its rich annotations of human activities, scene depth, and object masks, presents a promising foundation for future embodied pre-training.

4.2 Application: Human-centric World Modeling

This subsection evaluates the dataset’s utility for supervised end-to-end 4D reconstruction using Gaussian Splatting (GS). By providing high-quality RGB images, depth maps, and camera poses, WIYH supports shape and motion modeling for dynamic scenes. We extracted geometry using MegaSAM [33], tracked pixel trajectories of dynamic objects with TAPIR [14], and performed scene reconstruction with Shape of Motion [47]. The successful application of our dataset in spatial perception tasks like 4D Gaussian Splatting (4DGS) demonstrates the critical role of its rich annotations, particularly depth information, in enhancing spatial understanding and representation.

As shown in Table 3, photometric metrics remain relatively consistent, whereas geometric metrics vary notably across tasks. These differences highlight the inherent challenges in reconstructing dynamic scenes, where accurate geometry prediction is particularly complex in motion-rich environments. This observation suggests promising directions for future research in 4D reconstruction for robotic manipulation, particularly methods that improve geometric understanding in complex dynamic scenes.

Figure 7 presents the 4D reconstruction results at various time steps, showcasing the dataset’s potential for dynamic scene modeling. By capturing high-quality dynamic scenes, WIYH can help leverage Gaussian Splatting (GS) as

Table 3: Comparison of photometric and geometric metrics for different tasks.

Scene	Task	Photometry			Geometry	
		PSNR \uparrow	SSIM \uparrow	LPIPS \downarrow	A.R. \downarrow	$\delta_1\uparrow$
1	Pouring Wine	20.15	0.815	0.206	1.04	52.01
2	Packing Clothes	20.02	0.656	0.423	2.89	17.83
3	Packing Cargo	18.83	0.749	0.552	3.52	13.79

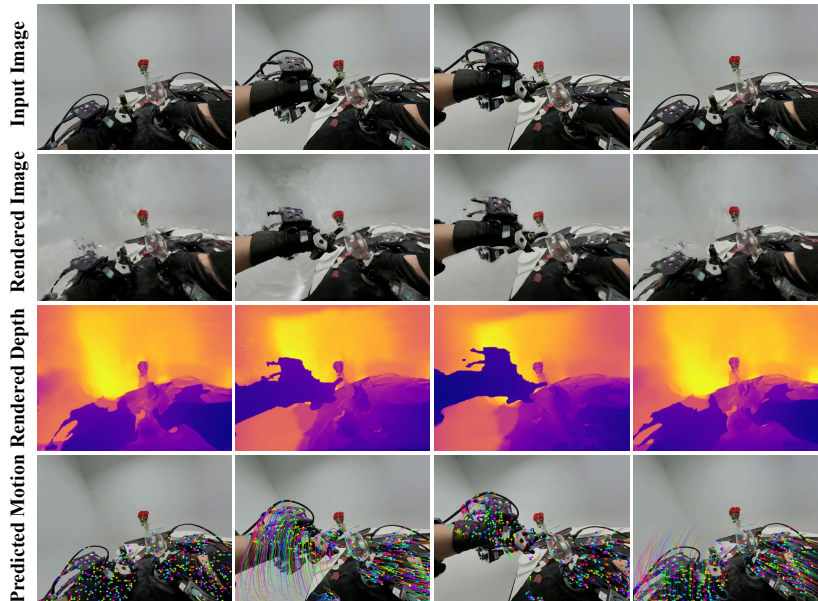


Fig. 7: 4D Reconstruction Result. For the pouring wine task, we present the 4DGS reconstruction results across multiple timestamps. The visualizations include the rendered image, estimated depth map, and predicted 4D motion field. The results demonstrate that our WIYH dataset enables clean and accurate 4D reconstruction, even in challenging, dynamic action scenarios.

an effective 3D tokenizer, advance spatial understanding, and enrich Real2Sim pipelines and neural-network-based simulation.

In addition, we further present the experimental results of video generation in the supplementary materials.

5 Human-centric Manipulation

5.1 Experiment Objective and Implementation

In this section, our objective is to validate the efficacy of the WIYH data collection system and dataset for robotics manipulation. To this end, we formulate two core research questions. (1) Does utilizing the WIYH dataset as pre-training

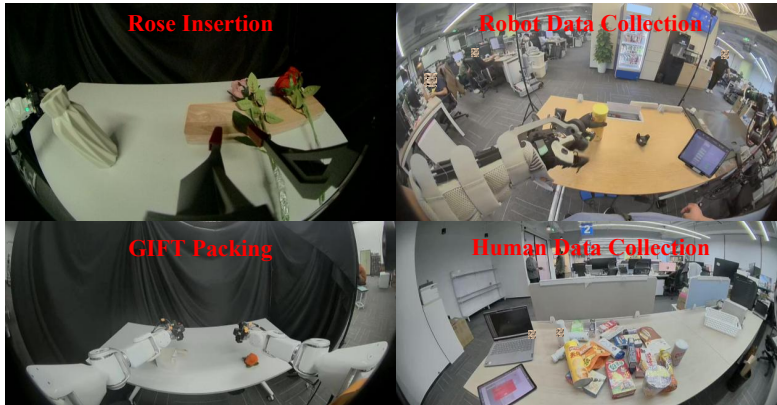


Fig. 8: Experiment setup. The left side demonstrates samples of rose insertion and gift packing in the cross-embodiment task. The right side shows data collection in the co-training task. Robot data contains single-object manipulation data starting from a limited set of initial poses, whereas human-centric data contains data from more complex scenes and covers a broader action space.

data enhance the embodied manipulation capabilities of the VLA model? **(2)** Does retargeting WIYH data to dexterous hand actions improve dexterous manipulation performance? To address these questions, we design two real-world manipulation experiments: **(1) cross-embodiment pretraining** and **(2) retargeting co-training**.

In the cross-embodiment pretraining experiment, we adopt StarVLA-PI [13] as the base model. We pre-train StarVLA-PI using WIYH data with atomic instruction annotations for both VLM and VLA data. For post-training, we select two tasks in a real-world environment: rose insertion and gift packing, and we collect 150 gripper-based teleoperation manipulation samples for each task, as shown on the left side of Figure 8. We compare the success rates across three settings, including VLM pre-training, VLA pre-training, and without pre-training. VLA pretraining refers to loading all pre-trained VLA weights during post-training, while VLM pretraining denotes loading only the VLM weights. During evaluation, each setting of each task is tested 10 times with object positions and target objects varied in each trial.

In the retargeting co-training experiment, we construct a combined dataset using UMI robot data D_r collected in constrained environments and data D_h of the same task collected using the Oracle Suite. The robot system employs a low-degree-of-freedom dexterous hand as the end-effector H , and the hand data from D_h is retargeted to match the degrees of freedom of H . We evaluate the effectiveness of the human-centric data collected by Oracle Suite across various dexterous grasping tasks. Implementation details will be provided in the supplementary materials. Notably, the right side of figure 8 shows scene examples and the data collection setup. The collected robot data D_r always starts from a limited number of initial poses in the single-object scene. In contrast,

Table 4: Comparison of real-world performance in cross-embodiment pretraining experiment.

Method	Rose Insertion	Gift Packing	AVG
w/o Pretrain	1/10	2/10	15%
VLM Pretrain	3/10	3/10	30%
VLA Pretrain	6/10	8/10	70%

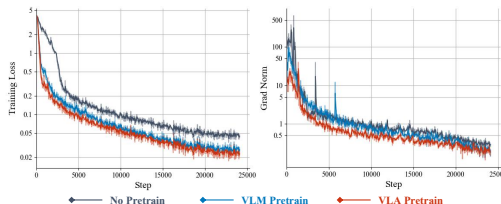


Fig. 9: Cross-embodiment pretrain loss.

human-centric data D_h contains only manipulation sequences from multi-object cluttered scenes, making a larger observation domain and action space than D_r .

5.2 Results and In-depth Discussion

In this section, we analyze the results of two experiments to demonstrate how WIYH empowers robotic manipulation.

For the cross-embodiment pretraining experiments, we demonstrate the quantitative result and the training loss in Table 4 and in Figure 9, respectively. As indicated by success rates, utilizing WIYH for VLA pre-training yields the most significant performance improvements, from 15% to 70%. Besides, as illustrated in Figure 9, VLA pre-training achieves lower loss and smoother gradient convergence than VLM pre-training and no pre-training. This efficacy remains robust given the cross-embodiment gap between the pre-training data (human hands) and post-training data (robot gripper).

For the retargeting co-training experiments, we demonstrate the quantitative and qualitative results in Table 5 and in Figure 10, respectively. In the single-object scenario, the robot arm begins execution from a random initial pose during testing, which differs from the initial pose used in the robot data D_r . In the multi-object cluttered scenario, we primarily evaluate the performance of the co-training strategy under conditions of varying scene height, changes in the target object’s pose, and increased occlusion. The configurations of these test scenarios and qualitative experimental results are illustrated in Figure 10. Quantitative results are summarized in Table 5. (1) In the single-object scenario, co-training the policy with both robot data and human-centric data leads to an improvement in the success rate of more than 13%. Although the motion precision in the human-centric data is limited, its diverse action distribution enhances the policy’s generalization capability to unseen initial states. (2) Policies trained solely on robot data exhibit minimal generalization capability in complex scenarios. Simply increasing data quantity from 200 clips to 500 clips yields marginal performance improvement from 0% to 8%. However, after co-training with human-centric data, the success rate increases by 52%. This demonstrates that incorporating human-centric data significantly improves the policy’s ability to interpret complex scenes. Therefore, the co-training approach effectively introduces both the action domain and observation domain of human-centric data into the robot dataset, thereby enhancing the generalization capability of the learned policy.

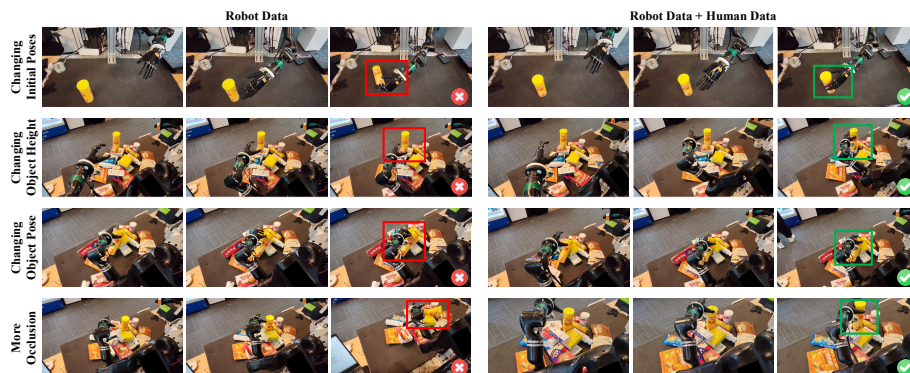


Fig. 10: Real-robot manipulation experiments. We present the comparison of manipulation policy performance under four novel task settings, where the policies are trained either exclusively on robot data collected or co-trained using both robot data and annotated human-centric data.

Table 5: A comparison of results on two manipulation scenarios trained with data from different sources is presented. The datasets include robot data and human-centric data. And the success rate (SR) was reported.

Scenario	Data Sources and Amounts (Clips)		SR (%)
	Robot data amount	Human data amount	
Single-object Scene	200	0	20
	200	800	23.3 (+3.3)
	500	0	43.3
	500	800	56.7 (+13.4)
Cluttered Scene	200	0	0.0
	200	800	32.0 (+32.0)
	500	0	8.0
	500	800	60.0 (+52.0)

6 Conclusion

In this paper, we present the WIYH ecosystem, a cornerstone for embodied intelligence research in real-world environments. We make three key contributions: the Oracle Suite, a wearable system enabling in-the-wild data capture with integrated markerless auto-labeling; the large-scale WIYH dataset, offering diverse, skilled human manipulation sequences with rich multimodal streams; and a suite of comprehensive benchmarks, supported by extensive atomic-action and vision-language annotations, for holistic evaluation from perception to physical interaction. Our benchmarks reveal that current models still lack the fine-grained spatial and causal reasoning required for robust embodied operation. The WIYH dataset, with its unique scale and rich annotations, is designed to bridge this gap. In the future, we will open-source the whole dataset and hardware design to promote human-centric manipulation research.

Appendix

A World In Your Hands Ecosystem

A.1 Hardware Details

Camera: We primarily use two fisheye cameras below each wrist and two fisheye cameras on the chest as the raw RGB signal sources. These cameras feature a 180° field of view with an original resolution of 1536 × 1920 pixels.

Tactile: We utilize resistive pressure sensors with a resolution of 5 mN and a range of 0.2 N to 50 N distributed across the fingertips of all fingers.

Autolabel Pipeline: The autolabeling pipeline involves online and offline algorithms. Specifically, the online localization module performs lightweight coarse positioning using visual-inertial odometry (VIO) algorithms [37] and IR detection, while the offline stage refines these coarse estimates through Structure-from-Motion (SfM) algorithms [40].

A.2 Data Collection Efficiency

The Oracle Suite pipeline follows a *Collection, Annotation, Inspection, Archiving* workflow for scalable data production. A single collector operating 8 hours per day generates approximately 1.8 TB of valid multimodal data. At scale, 100 collectors over 30 days yield roughly 5.4 PB of raw data (stored in cloud repositories). Efficiency is further improved through standardized capture protocols and automated cloud-based annotation.

We compare the efficiency of different data collection paradigms in Table 6. Efficiency: taking the rose insertion task in our experiments as an example, given 8 hours as collection time, teleoperation can collect about 150 data clips; UMI-like methods, such as DexUMI [54], can collect about 400 data clips; our oracle suite can collect 720 data clips; and VR can collect around 800 data clips. Quality: VR-based hand tracking only provides 2D hand skeletons and suffers from visual occlusion. In contrast. In comparison, the Oracle Suite provides accurate 3D hand skeletons, even if under visual occlusion.

Table 6: Comparison of dexterous data collection paradigms.

	Teleop	DexUMI	VR	Oracle Suit (Ours)
Efficiency	☆☆☆☆☆	★☆☆☆☆	★★★★☆	★★★★☆
Quality	★★★★☆	★★★★☆	★☆☆☆☆	★★★★☆
End-effector	Dexterous	Dexterous	Hands	Hands

B World In Your Hands Dataset

B.1 Detailed Task-Skill Counting Statistics

- We further supplement the visualization of the number of skills corresponding to each task. Due to space limitations, we report statistics based on only 25% of the dataset, as shown in Figure 11. Please zoom in electronically to inspect the details. The full visualization analysis will be updated subsequently on the dataset website.



Fig. 11: Task-skill count visualization of 25% dataset.

B.2 Data Annotation Details.

Raw videos are structured into a three-tier hierarchy: Scene - Task - Subtask by annotators. Each subtask corresponds to the minimal object-centered action unit or a temporally cohesive action sequence. **(1) Atomic (Subtask) Annotation:**

- **Actions (Skills):** Drawn from predefined operation sets (e.g., PICK, PLACE INTO, SEARCH).
- **Target Object:** Semantic structure describing objects (e.g., [cloth, container]).

- **Temporal Bounds:** Precise start/end timestamps delimiting the execution segment in the video.
- **Status:** Labeled as success, failure, irrelevant to denote execution outcome.

(2) **Chain-of-Thought (CoT) Reasoning:** With the subtask annotation, we select tasks of moderate length (containing 4-10 subtasks). We annotate them with Chain-of-Thought data, providing reasoning that decomposes the task into several logically connected subtasks. The annotation pipeline for CoT is illustrated in Figure 12. Initially, we provide the model (Qwen2.5-VL-72B [3]) with both the current subtask information (video and subtask instruction) and the ground-truth instruction of the next subtask. The model is then prompted to perform posterior attribution, explaining why the specified next subtask logically follows. Subsequently, the attribution is appended to the input and presented again to Qwen2.5-VL-72B, synthesizing it into a structured causal reasoning process. Next, the CoT segment is extracted and used to prompt Qwen3 [55], which is instructed to predict an answer. This predicted answer is matched against the ground-truth answer to automatically validate the completeness and soundness of the CoT labeling. Finally, human review and correction of erroneous annotations are performed.

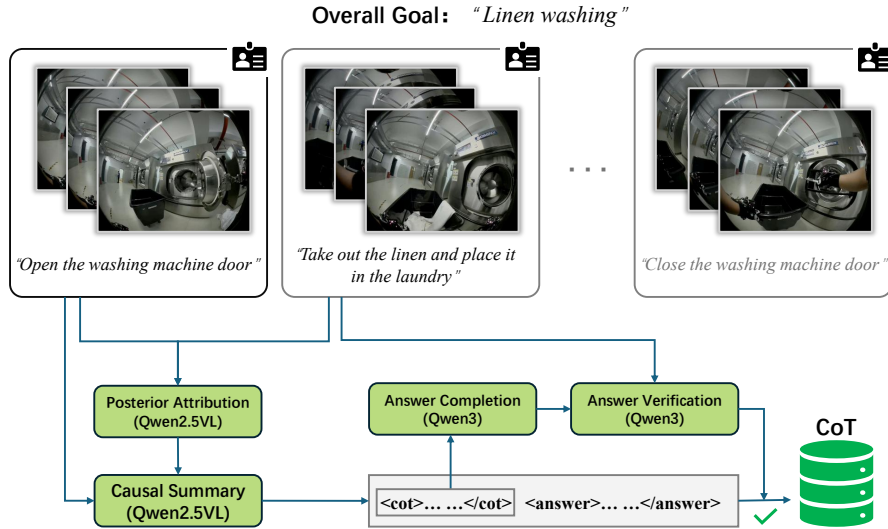


Fig. 12: The annotation pipeline for subtask prediction chain-of-thought (CoT).

B.3 More visualization.

We present more visualizations about the annotations of our dataset in Figure 13. Annotations of the Human-centric Vision-Language tasks are shown in Figure 14.

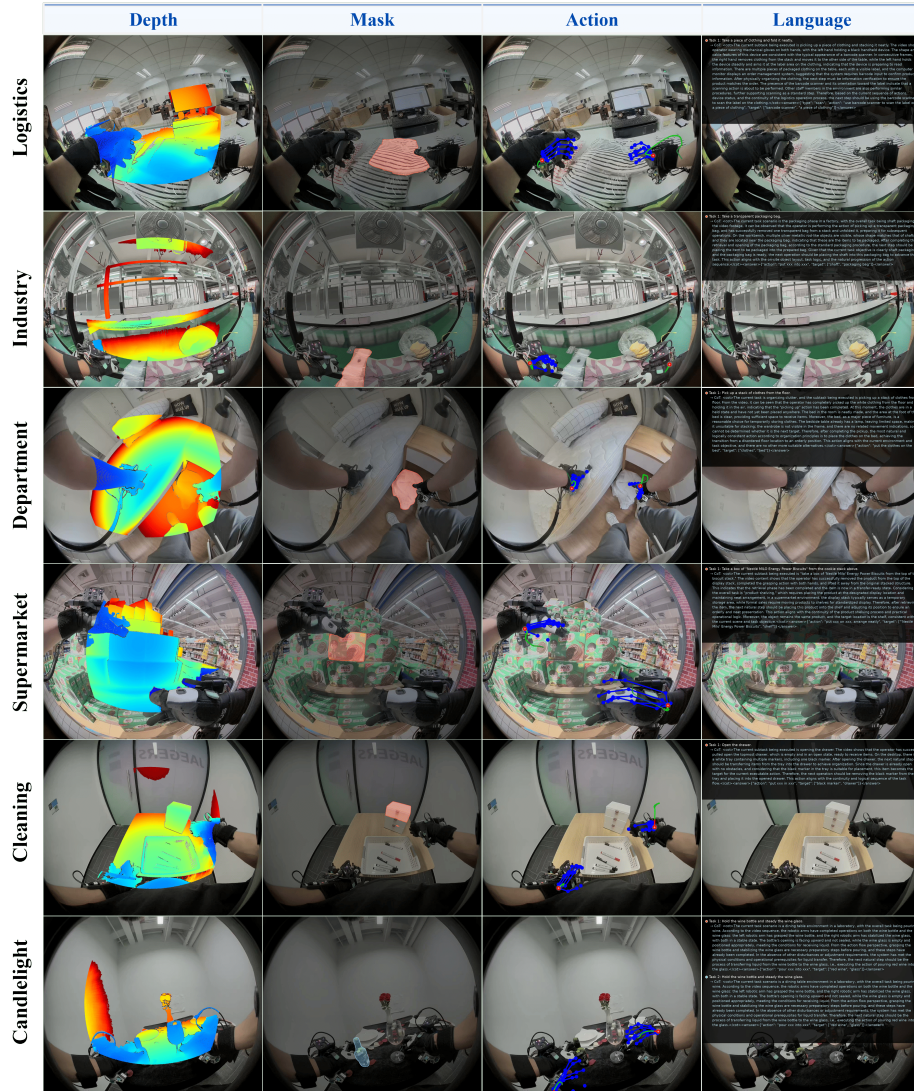


Fig. 13: Data annotation samples cross different scenes. The example of human-centric data annotations, including depth, mask, action, and task descriptions, in six different scenarios.

TASK: Spatial Referring



Q: Identify several spots within the vacant space that's on the desktop between the two documents. Your answer should be formatted as a list of tuples, i.e. [(x1, y1), (x2, y2), ...], where each tuple contains the x and y coordinates of a point satisfying the conditions above. The coordinates should be between 0 and 1, indicating the normalized pixel locations of the points in the image.



Q: Identify several spots within the vacant space that's on the surface of the black rectangular conveyor belt beneath the second television. Your answer should be formatted as a list of tuples, i.e. [(x1, y1), (x2, y2), ...], where each tuple contains the x and y coordinates of a point satisfying the conditions above. The coordinates should be between 0 and 1, indicating the normalized pixel locations of the points in the image.



Q: Identify several spots within the vacant space that's on the tabletop between a stack of linens on the left and a stack of linens on the right. Your answer should be formatted as a list of tuples, i.e. [(x1, y1), (x2, y2), ...], where each tuple contains the x and y coordinates of a point satisfying the conditions above. The coordinates should be between 0 and 1, indicating the normalized pixel locations of the points in the image.



Q: Identify several spots within the vacant space that's on the countertop in front of the kettle and tea set on the bar. Your answer should be formatted as a list of tuples, i.e. [(x1, y1), (x2, y2), ...], where each tuple contains the x and y coordinates of a point satisfying the conditions above. The coordinates should be between 0 and 1, indicating the normalized pixel locations of the points in the image.



Q: Identify several spots within the vacant space that's on the surface of the green chair. Your answer should be formatted as a list of tuples, i.e. [(x1, y1), (x2, y2), ...], where each tuple contains the x and y coordinates of a point satisfying the conditions above. The coordinates should be between 0 and 1, indicating the normalized pixel locations of the points in the image.



Q: Identify several spots within the vacant space that's on the chair near the right-side window. Your answer should be formatted as a list of tuples, i.e. [(x1, y1), (x2, y2), ...], where each tuple contains the x and y coordinates of a point satisfying the conditions above. The coordinates should be between 0 and 1, indicating the normalized pixel locations of the points in the image.

TASK: Subtask Prediction



The overall goal is to - Product labeling and sorting check. The agent in the video is currently performing the subtask - Tear off a label - to complete this goal. For the agent in the video, what is the most plausible next immediate subtask from the choices below?

"A": "Lift the packing paper and place it in the leftmost shoebox unbranded area",
 "B": "Stick a label on the leftmost shoebox unbranded area",
 "C": "Stick a label on the surface of the tool bag",
 "D": "Place the toolbox in the leftmost shoebox unbranded area"



The overall goal is to - Linen washing. The agent in the video is currently performing the subtask - Take out a piece of linen from the linen cart and put it in the washing machine - to complete this goal. For the agent in the video, what is the most plausible next immediate subtask from the choices below?

"A": "Close the washing machine door",
 "B": "Push the washing machine door to one side",
 "C": "Close the laundry basket lid",
 "D": "Open the washing machine door"

TASK: Completion Verification



The agent in the video was given the task - Product packing for outbound. To make progress towards the instruction, the agent attempted to complete the following subtask - Seal the cardboard box with tape. Was it successful in completing this subtask?

A:Yes B:No



The agent in the video was given the task - Linen folding and shaping. To make progress towards the instruction, the agent attempted to complete the following subtask - Unfold the towel and stack it on top of the folded towels. Was it successful in completing this subtask?

A:Yes B:No

Fig. 14: Examples of annotations in the Human-centric Vision-Language Benchmark.

C Benchmark And Application Details

C.1 Human-centric Vision-Language

Benchmark Task Descriptions. The Human-centric Vision-Language Benchmark in Section 4.1 is constructed by sampling raw data from WIYH, followed by manual annotation, including Spatial Referring, Subtask Prediction, and Completion Verification, with the amounts and distributions illustrated in Figure 15. In these tasks, all VLMs are directly tested without any training.

(1) The Spatial Referring is designed as a spatial region grounding form: given relevant image frames, annotators delineate ROI areas using polygons according to the given questions. Specifically, given the question as prompts, the VLM outputs a set of points P_a representing the spatial region referenced in the question. We denote the set of points that fall within the ground-truth region as P_r . We evaluate the VLM’s spatial understanding by computing the proportion of the points that fall within the ground-truth region.

$$score_{SR} = \frac{N_a}{N_r}, \quad (1)$$

where N_a is the number of P_a and N_r is the number of P_r . $score_{SR}$ is a scalar in the range $[0, 1]$, with values closer to 1 indicating stronger spatial understanding capability of the VLM. This task is designed to evaluate the capability of VLM models to understand spatial referring in human-centric scenarios.

(2) The Subtask Prediction adopts a multiple-choice question format. We use the Qwen2.5-VL-72B tool to first generate nine negative candidate options based on video clips and ground truth values, covering both action and target object dimensions. Then, the annotators manually select three reasonable negative samples that fit the current scenario. These samples, along with the correct answers, constitute the final candidate set. That is, each question has four options, and the accuracy of random selection was approximately 25%. This task is designed to evaluate the capability of VLM models to perform long-horizon task planning and decomposition in human-centric scenarios.

(3) The Completion Verification is designed as binary questions: given a video segment randomly truncated from the end, annotators determine whether the subtask has been completed. The evaluation metric is the selection accuracy rate. The accuracy of random selection was approximately 50%. This task is designed to evaluate the capability of VLM models to understand the dynamic process of manipulation tasks in human-centric scenarios.

Tasks Visualization. We show the samples and detailed annotations of the three tasks in Figure 16.

Case Analysis. Figure 16 presents the results of the Qwen3-VL model on the Spatial Referring task. We observe that existing VLMs perform reasonably well on in-plane spatial referring relations (e.g., “between A and B” as illustrated in

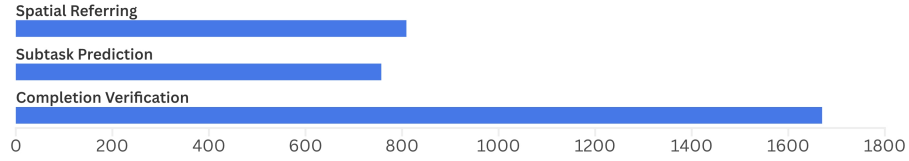


Fig. 15: Amount of three task annotations in the Human-centric Vision-Language Benchmark.

the first row). However, when it comes to relations that require understanding positions across different height levels, such as “beneath” or “between A and B” where A and B are situated at different heights, the models fail to grasp the correct spatial information.



Fig. 16: Case analysis of the Spatial Referring task.

C.2 Human-centric World Model

Gaussian Splatting 4D Reconstruction Evaluation Metrics. In terms of metrics of 4D reconstruction, we evaluate the RGB rendering quality using PSNR, SSIM, and LPIPS. For PSNR and SSIM, higher is better, while for LPIPS, lower is better. For geometry accuracy from rendered depth maps, we use A.R. (lower is better) and δ_1 (higher is better).

- PSNR (Peak Signal-to-Noise Ratio),

$$\text{PSNR} = 10 \cdot \log_{10} \left(\frac{\text{MAX}_I^2}{\text{MSE}} \right)$$

$$\text{MSE} = \frac{1}{MN} \sum_{i=1}^M \sum_{j=1}^N (I(i, j) - K(i, j))^2,$$

where I is the reference image, K is the rendered image, and MAX_I is the maximum possible pixel value. A higher PSNR indicates that the rendered image is closer to the ground truth.

- SSIM (Structural Similarity Index Measure).

$$\text{SSIM}(x, y) = \frac{(2\mu_x\mu_y + c_1)(2\sigma_{xy} + c_2)}{(\mu_x^2 + \mu_y^2 + c_1)(\sigma_x^2 + \sigma_y^2 + c_2)},$$

where μ , σ , and σ_{xy} denote the mean, variance, and covariance of image patches x and y , respectively. SSIM evaluates perceptual similarity in terms of luminance, contrast, and structure; values closer to 1 indicate better similarity.

- LPIPS (Learned Perceptual Image Patch Similarity). This metric computes the perceptual distance between rendered and ground-truth images by extracting deep features from a pretrained CNN and measuring the distance in that feature space. Lower LPIPS values indicate that two images are more perceptually similar.
- AbsRel (Absolute Relative Error).

$$\text{AbsRel} = \frac{1}{N} \sum_{i=1}^N \frac{|d_i - d_i^*|}{d_i^*},$$

where d_i is the predicted depth at the pixel i and d_i^* is the corresponding ground-truth depth. A lower value denotes a more accurate geometry.

- δ_1 (Threshold Accuracy / Delta1).

$$\delta_1 = \frac{1}{N} \sum_{i=1}^N \mathbf{1} \left(\max \left(\frac{d_i}{d_i^*}, \frac{d_i^*}{d_i} \right) < 1.25 \right),$$

which measures the percentage of predicted depth values that are within a factor of 1.25 of the ground-truth depth. A higher value δ_1 indicates better accuracy.

During optimization, all input videos are processed at a resolution of 960×720 . We represent each scene with 40k dynamic Gaussians and 100k static Gaussians and use $B = 10$ shared SE(3) motion bases for all points. We optimize the model with Adam, running 1k iterations for the initialization stage and 500 training epochs, with learning rates of 1.6×10^{-4} for Gaussian means and SE(3) bases, 5×10^{-3} for scales, 1×10^{-3} for rotations, and 1×10^{-2} for colors, opacities, and motion coefficients. Training on a 300-frame sequence takes about 2 hours on a single A100 GPU and supports real-time rendering at around 140 FPS.

Addition Application: Language-conditioned Video Generation This section evaluates the contribution of our proposed WIYH dataset to enhancing video generation performance in human-centric manipulation tasks. We fine-tuned two baseline models, transformer-based CogVideo [19] and UNet-based DynamiCrafter [52], initialized with their original weights, using WIYH under the image-and-text-to-video setting. During fine-tuning, all input videos were resized to 480p resolution. We randomly select 90% of the data as the training set and the remaining 10% as the test set.

As shown in Figure 17, models fine-tuned with WIYH generate egocentric videos with improved spatial and temporal coherence, as well as stronger alignment with both the input image and action instructions. For example, in the “Wipe the cabinet” task, the cabinet’s orientation and the towel’s color are reproduced more accurately. In contrast, videos generated by non-fine-tuned models exhibit noticeable object fragmentation and distortion, along with discontinuous and physically implausible hand-object interactions. Notably, after fine-tuning, the complex motions of non-rigid objects in the generated videos appear more realistic and natural. These improvements demonstrate that WIYH substantially enhances a model’s ability to capture real-world dynamics.

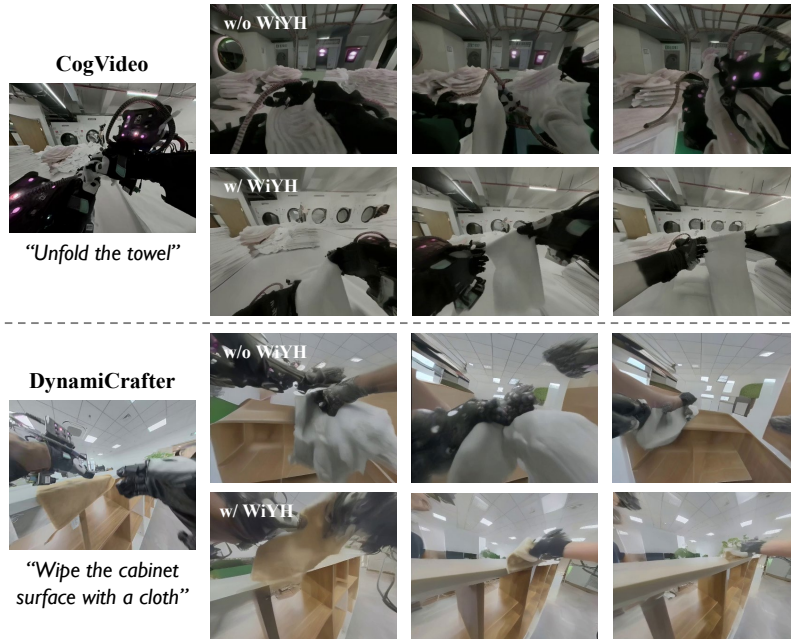


Fig. 17: Language-Conditioned Video Generation. When provided with language instructions, two baseline video prediction methods exhibited significant hallucinations without WIYH fine-tuning. However, after fine-tuning on our dataset, they demonstrated a markedly enhanced ability to imagine future states.

Quantitative results are summarized in Table 7. We use four metrics from VBench [22]—consistency, smoothness, dynamic (motion intensity), and quality in order to assess motion plausibility, temporal coherence, and visual fidelity of the video generation models. Following VBench [22], the evaluation metrics are as follows:

- **Consistency.** To evaluate the temporal consistency of the target manipulation subjects, we calculate the DINO [10] feature similarity across frames. For assessing the temporal consistency of the background scenes, we compute the CLIP [38] feature similarity across frames. The overall consistency score is defined as the arithmetic mean of the subject consistency and the background consistency.
- **Smoothness.** To assess the temporal continuity of the generated videos, we employ a motion-consistency metric based on the AMT [32] video frame interpolation model. Given a generated video with frames $\{f_0, f_1, \dots, f_{2n-1}, f_{2n}\}$, we first remove all odd-indexed frames to obtain $\{f_0, f_2, \dots, f_{2n}\}$. The AMT model is then used to interpolate the missing frames, producing $\{\hat{f}_1, \hat{f}_3, \dots, \hat{f}_{2n-1}\}$. Finally, we compute the mean absolute error between the interpolated and original frames, where a larger value indicates smoother and more temporally coherent motion.
- **Dynamic.** To prevent the model from producing static videos in pursuit of higher temporal consistency scores, we employ RAFT [41] to estimate optical flow strengths between consecutive frames of each generated video. The average of the largest 5% optical flows is used to determine whether the video is static. The final dynamic score is calculated by measuring the proportion of non-static videos generated by the model.
- **Quality.** To assess the visual quality of generated video frames, we employ the MUSIQ [25] image quality predictor trained on the SPAQ [15] dataset. This metric quantifies common distortions such as overexposure, noise, and blur, with a higher score indicating fewer artifacts.

After fine-tuning with the WIYH dataset, both baseline models show clear improvements across all metrics, with the most significant gains observed in dynamics and temporal consistency.

Table 7: Comparison of consistency, smoothness, dynamics, and quality metrics under different conditions.

Metric	CogVideo		DyamiCrafter	
	w/o WIYH	w/ WIYH	w/o WIYH	w/ WIYH
Consistency \uparrow	80.6	88.2 (+7.6)	85.3	91.5 (+6.2)
Smoothness \uparrow	93.5	98.4 (+4.9)	97.4	98.6 (+1.2)
Dynamic \uparrow	62.9	78.5 (+15.6)	74.8	89.6 (+14.8)
Quality \uparrow	60.1	67.6 (+7.5)	63.5	70.6 (+7.1)

D Details of Human-centric Manipulation

In this section, we present the details of our co-training experiments in Section 5, Human-centric Manipulation, of the main text. As shown in Figure 18, we demonstrate 11 task variants under two scenarios: Single-Object Scene and Multi-Object Cluttered Scene. Figures 19 and 20 illustrate the success rates and failure causes for each task in these two scenarios, respectively.

As shown in Figures 19 and 20, on most tasks, the incorporation of human data leads to a general increase in success rate. In the Single-Object Scene, the diverse action distribution of human data enhanced the policy’s generalization capability to unseen initial states, enabling successful grasping at different positions or over long distances. In the Multi-Object Cluttered Scene, policies trained solely on robot data demonstrated almost no generalization ability in complex scenarios. When factors such as object height or layout changed, policies trained only on robot data failed, whereas the inclusion of human data gradually enabled success by effectively introducing both the action and observation domains of human data into the robot dataset. Furthermore, the consistently low success rates across all methods in certain tasks highlight important directions for future research: how to further improve the collection precision of human data and how to design efficient algorithms that can better transfer knowledge from human data to dexterous manipulation tasks.



Fig. 18: Task variant visualization in the co-training experiment.

E Ethics and Privacy Statement

Our work involves large-scale data collection of real-world human manipulation activities. We took a number of measures to ensure responsible data handling, privacy protection, and ethical compliance.

Data Collection and Consent. All human subjects participating in data collection were recruited voluntarily and provided informed consent in accordance with institutional guidelines. Participants were briefed on the purpose of the study, the modalities collected (RGB video, depth, motion capture, tactile sensing), the intended research use, and their right to withdraw at any time.

Privacy Protection. Although the dataset contains real-world human activities and may capture visible human faces or identifiable biometric patterns, several privacy-preserving strategies were implemented:

- **Controlled subjects only:** No bystanders or non-consenting individuals appear in the dataset; all scenes were recorded in controlled environments with only consenting operators present.
- **No identity labels:** We do not include personal information, demographic information, or identity annotations.
- **Face and identity protection:** When faces are visible in RGB streams, we apply optional face blurring in the public release version.
- **No audio recordings:** We do not collect speech or audio signals to avoid unintended disclosure of personal information.

Sensitive Content and Safety. The dataset does not include minors, hazardous behaviors, or sensitive activities. All recordings were conducted in standard workplace or daily-life environments using safety protocols.

Data Usage and Licensing. The released dataset is intended exclusively for research on embodied AI, manipulation, perception, and VLA learning. Redistribution or commercial use is restricted according to the license accompanying the dataset. Users are required to comply with ethical research practices and avoid any attempts at identity recognition or misuse of human-related data.

Potential Risks and Mitigations. As with any dataset containing human recordings, there is a theoretical risk of model misuse, such as identity extraction or surveillance applications. To mitigate these risks, we provide: (1) no textual identity metadata, (2) optional visual anonymization tools, and (3) a license that explicitly forbids re-identification, face recognition, or surveillance-related uses.

Institutional Review. All data collection procedures were reviewed and approved by an internal ethics committee to ensure compliance with privacy protection and responsible AI principles.

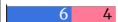
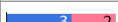
Task Variation	Training Recipe	Failure Analysis	Success vs. Failure
(1) Grasping from HOME_POINT with the target in front of hand.	UMI#200	Failed to reach a reasonable position, early grasping	 6 4
	UMI#500	Grasped air	 9 1
	UMI#200+WiyH#800	Failed to reach a reasonable position, early grasping	 6 4
	UMI#500+WiyH#800	-	 10
(2) Grasping from HOME_POINT with the target in right, front of hand.	UMI#200	Far distance, can not grasping	 5
	UMI#500	Failed to reach a reasonable position, early grasping	 5
	UMI#200+WiyH#800	Failed to reach a reasonable position, early grasping	 5
	UMI#500+WiyH#800	Failed to reach a reasonable position, early grasping	 3 2
(3) Grasping from HOME_POINT with the target in right, front of hand, away from hand.	UMI#200	Large positional deviation	 5
	UMI#500	Significant deviation from the target	 5
	UMI#200+WiyH#800	Failed to reach a reasonable position, collided with target	 5
	UMI#500+WiyH#800	Reached the position, unreasonable grasp timing	 1 4
(4) Grasping from HOME_POINT with the target in middle of platform, parallel to the hand.	UMI#200	Unable to reach the grasping position	 5
	UMI#500	Unable to reach the grasping position	 5
	UMI#200+WiyH#800	Collided with the target	 5
	UMI#500+WiyH#800	Failed to reach a reasonable position, early grasping, collided	 5
(5) Grasping from HOME_POINT with the target in left of hand, close to the hand.	UMI#200	Collided with the target	 5
	UMI#500	Severe finger compression	 3 2
	UMI#200+WiyH#800	Collided with the target	 5
	UMI#500+WiyH#800	Failed to reach a reasonable position, early grasping, collided	 3 2
(6) Hand facing to the target directly.	UMI#200	Joint and motion anomalies	 5
	UMI#500	Failed to reach a reasonable position, early grasping, collided	 1 4
	UMI#200+WiyH#800	Collided with the target	 1 4
	UMI#500+WiyH#800	Collided with the target	 5

Fig. 19: Dexterous manipulation Details - 1.

Task Variation	Training Recipe	Failure Analysis	Success vs. Failure
(7) Crowded objects around the target.	UMI#200	Abnormal grasping behavior	 5
	UMI#500	Failed to reach a reasonable position, early grasping, collided	 2 3
	UMI#200+WiYH#800	Failed to reach a reasonable position, early grasping, collided	 3 2
	UMI#500+WiYH#800	Failed to reach a reasonable position, early grasping, collided	 4 1
(8) Obstacle in front of the target.	UMI#200	Abnormal grasping behavior	 5
	UMI#500	Unable to reach the target position	 5
	UMI#200+WiYH#800	Grasping position too low, collided with other assets	 2 3
	UMI#500+WiYH#800	Severe finger compression	 3 2
(9) Elevated the target.	UMI#200	Abnormal grasping behavior	 5
	UMI#500	Unable to reach the grasping position	 5
	UMI#200+WiYH#800	Reached the grasping position, grasping failed	 3 2
	UMI#500+WiYH#800	Severe finger compression	 5
(10) Elevated the target, hand facing to the target directly.	UMI#200	Unable to reach the grasping position	 5
	UMI#500	Unable to reach the grasping position	 5
	UMI#200+WiYH#800	Failed to reach a reasonable position, early grasping	 5
	UMI#500+WiYH#800	-	 5
(11) leaned target.	UMI#200	Unable to reach the grasping position	 5
	UMI#500	Incorrect grasping location	 5
	UMI#200+WiYH#800	Incorrect grasping location	 5
	UMI#500+WiYH#800	Incorrect grasping location	 3 2

Fig. 20: Dexterous manipulation Details - 2.

References

1. Achiam, J., Adler, S., Agarwal, S., Ahmad, L., Akkaya, I., Aleman, F.L., Almeida, D., Altenschmidt, J., Altman, S., Anadkat, S., et al.: Gpt-4 technical report. arXiv preprint arXiv:2303.08774 (2023)
2. Alayrac, J.B., Donahue, J., Luc, P., Miech, A., Barr, I., Hasson, Y., Lenc, K., Mensch, A., Millican, K., Reynolds, M., et al.: Flamingo: a visual language model for few-shot learning. *Advances in neural information processing systems* **35**, 23716–23736 (2022)
3. Bai, S., Chen, K., Liu, X., Wang, J., Ge, W., Song, S., Dang, K., Wang, P., Wang, S., Tang, J., Zhong, H., Zhu, Y., Yang, M., Li, Z., Wan, J., Wang, P., Ding, W., Fu, Z., Xu, Y., Ye, J., Zhang, X., Xie, T., Cheng, Z., Zhang, H., Yang, Z., Xu, H., Lin, J.: Qwen2.5-vl technical report. arXiv preprint arXiv:2502.13923 (2025)
4. Bai, Y., Chen, H., Chen, J., Chen, Z., Deng, Y., Dong, X., Hantrakul, L., Hao, W., Huang, Q., Huang, Z., et al.: Seed-music: A unified framework for high quality and controlled music generation. arXiv preprint arXiv:2409.09214 (2024)
5. Banerjee, P., Shkodrani, S., Moulon, P., Hampali, S., Han, S., Zhang, F., Zhang, L., Fountain, J., Miller, E., Basol, S., et al.: Hot3d: Hand and object tracking in 3d from egocentric multi-view videos. In: *Proceedings of the Computer Vision and Pattern Recognition Conference*. pp. 7061–7071 (2025)
6. Black, K., Brown, N., Driess, D., Esmail, A., Equi, M., Finn, C., Fusai, N., Groom, L., Hausman, K., Ichter, B., et al.: $\pi 0$: A vision-language-action flow model for general robot control. corr, abs/2410.24164, 2024. doi: 10.48550. arXiv preprint ARXIV.2410.24164
7. Brohan, A., Brown, N., Carbajal, J., Chebotar, Y., Dabis, J., Finn, C., Gopalakrishnan, K., Hausman, K., Herzog, A., Hsu, J., et al.: Rt-1: Robotics transformer for real-world control at scale. arXiv preprint arXiv:2212.06817 (2022)
8. Brown, T., Mann, B., Ryder, N., Subbiah, M., Kaplan, J.D., Dhariwal, P., Neelakantan, A., Shyam, P., Sastry, G., Askell, A., et al.: Language models are few-shot learners. *Advances in neural information processing systems* **33**, 1877–1901 (2020)
9. ByteDance Doubao Team: Doubao seed 1.6-vision: A hybrid-training vision-language model (2024), <https://modelscope.cn/models/doubao-seed-1.6-vision>, accessed: 2025-11-14
10. Caron, M., Touvron, H., Misra, I., Jégou, H., Mairal, J., Bojanowski, P., Joulin, A.: Emerging properties in self-supervised vision transformers. In: *Proceedings of the IEEE/CVF international conference on computer vision*. pp. 9650–9660 (2021)
11. Chao, Y.W., Yang, W., Xiang, Y., Molchanov, P., Handa, A., Tremblay, J., Narang, Y.S., Van Wyk, K., Iqbal, U., Birchfield, S., et al.: Dexycb: A benchmark for capturing hand grasping of objects. In: *Proceedings of the IEEE/CVF conference on computer vision and pattern recognition*. pp. 9044–9053 (2021)
12. Chowdhery, A., Narang, S., Devlin, J., Bosma, M., Mishra, G., Roberts, A., Barham, P., Chung, H.W., Sutton, C., Gehrmann, S., et al.: Palm: Scaling language modeling with pathways. *Journal of Machine Learning Research* **24**(240), 1–113 (2023)
13. starVLA Contributors: Starvla: A lego-like codebase for vision-language-action model developing. GitHub repository (1 2025). <https://doi.org/10.5281/zenodo.18264214>, <https://github.com/starVLA/starVLA>
14. Doersch, C., Yang, Y., Vecerik, M., Gokay, D., Gupta, A., Aytar, Y., Carreira, J., Zisserman, A.: Tapir: Tracking any point with per-frame initialization and temporal refinement. In: *Proceedings of the IEEE/CVF International Conference on Computer Vision*. pp. 10061–10072 (2023)

15. Fang, Y., Zhu, H., Zeng, Y., Ma, K., Wang, Z.: Perceptual quality assessment of smartphone photography. In: Proceedings of the IEEE/CVF conference on computer vision and pattern recognition. pp. 3677–3686 (2020)
16. Grauman, K., Westbury, A., Byrne, E., Chavis, Z., Furnari, A., Girdhar, R., Hamburger, J., Jiang, H., Liu, M., Liu, X., et al.: Ego4d: Around the world in 3,000 hours of egocentric video. In: Proceedings of the IEEE/CVF conference on computer vision and pattern recognition. pp. 18995–19012 (2022)
17. Grauman, K., Westbury, A., Torresani, L., Kitani, K., Malik, J., Afouras, T., Ashutosh, K., Baiyya, V., Bansal, S., Boote, B., et al.: Ego-exo4d: Understanding skilled human activity from first-and third-person perspectives. In: Proceedings of the IEEE/CVF Conference on Computer Vision and Pattern Recognition. pp. 19383–19400 (2024)
18. He, Y., Liang, S., Rui, X., Cai, C., Wan, G.: Egovm: Achieving precise ego-localization using lightweight vectorized maps. In: 2024 IEEE/RSJ International Conference on Intelligent Robots and Systems (IROS). pp. 12248–12255. IEEE (2024)
19. Hong, W., Ding, M., Zheng, W., Liu, X., Tang, J.: Cogvideo: Large-scale pretraining for text-to-video generation via transformers. In: The Eleventh International Conference on Learning Representations (2022)
20. Hoque, R., Huang, P., Yoon, D.J., Sivapurapu, M., Zhang, J.: Egodex: Learning dexterous manipulation from large-scale egocentric video. arXiv preprint arXiv:2505.11709 (2025)
21. Hsieh, J., Tu, K.H., Hung, K.H., Ke, T.W.: Dexman: Learning bimanual dexterous manipulation from human and generated videos. arXiv preprint arXiv:2510.08475 (2025)
22. Huang, Z., He, Y., Yu, J., Zhang, F., Si, C., Jiang, Y., Zhang, Y., Wu, T., Jin, Q., Chanpaisit, N., et al.: Vbench: Comprehensive benchmark suite for video generative models. In: Proceedings of the IEEE/CVF Conference on Computer Vision and Pattern Recognition. pp. 21807–21818 (2024)
23. Hurst, A., Lerer, A., Goucher, A.P., Perelman, A., Ramesh, A., Clark, A., Ostrow, A., Welihinda, A., Hayes, A., Radford, A., et al.: Gpt-4o system card. arXiv preprint arXiv:2410.21276 (2024)
24. Kareer, S., Patel, D., Punamiya, R., Mathur, P., Cheng, S., Wang, C., Hoffman, J., Xu, D.: Egomimic: Scaling imitation learning via egocentric video. In: 2025 IEEE International Conference on Robotics and Automation (ICRA). pp. 13226–13233. IEEE (2025)
25. Ke, J., Wang, Q., Wang, Y., Milanfar, P., Yang, F.: Musiq: Multi-scale image quality transformer. In: Proceedings of the IEEE/CVF international conference on computer vision. pp. 5148–5157 (2021)
26. Kim, M.J., Pertsch, K., Karamcheti, S., Xiao, T., Balakrishna, A., Nair, S., Rafailov, R., Foster, E., Lam, G., Sanketi, P., et al.: Openvla: An open-source vision-language-action model. arXiv preprint arXiv:2406.09246 (2024)
27. Kirillov, A., Mintun, E., Ravi, N., Mao, H., Rolland, C., Gustafson, L., Xiao, T., Whitehead, S., Berg, A.C., Lo, W.Y., Dollár, P., Girshick, R.: Segment anything. arXiv:2304.02643 (2023)
28. Kwon, T., Tekin, B., Stühmer, J., Bogo, F., Pollefeys, M.: H2o: Two hands manipulating objects for first person interaction recognition. In: Proceedings of the IEEE/CVF international conference on computer vision. pp. 10138–10148 (2021)
29. Li, F., Zhang, R., Zhang, H., Zhang, Y., Li, B., Li, W., Ma, Z., Li, C.: Llava-next-interleave: Tackling multi-image, video, and 3d in large multimodal models. arXiv preprint arXiv:2407.07895 (2024)

30. Li, J., Li, D., Savarese, S., Hoi, S.: Blip-2: Bootstrapping language-image pre-training with frozen image encoders and large language models. In: International conference on machine learning. pp. 19730–19742. PMLR (2023)
31. Li, J., Li, D., Xiong, C., Hoi, S.: Blip: Bootstrapping language-image pre-training for unified vision-language understanding and generation. In: International conference on machine learning. pp. 12888–12900. PMLR (2022)
32. Li, Z., Zhu, Z.L., Han, L.H., Hou, Q., Guo, C.L., Cheng, M.M.: Amt: All-pairs multi-field transforms for efficient frame interpolation. In: Proceedings of the IEEE/CVF Conference on Computer Vision and Pattern Recognition. pp. 9801–9810 (2023)
33. Li, Z., Tucker, R., Cole, F., Wang, Q., Jin, L., Ye, V., Kanazawa, A., Holynski, A., Snavely, N.: Megasam: Accurate, fast and robust structure and motion from casual dynamic videos. In: Proceedings of the Computer Vision and Pattern Recognition Conference. pp. 10486–10496 (2025)
34. Liu, Y., Liu, Y., Jiang, C., Lyu, K., Wan, W., Shen, H., Liang, B., Fu, Z., Wang, H., Yi, L.: Hoi4d: A 4d egocentric dataset for category-level human-object interaction. In: Proceedings of the IEEE/CVF Conference on Computer Vision and Pattern Recognition. pp. 21013–21022 (2022)
35. OpenAI: Gpt-4o: The omni model. Tech. rep. (May 2024), <https://openai.com/index/hello-gpt-4o>, accessed: 2025-11-14
36. Peddi, R., Arya, S., Challa, B., Pallapothula, L., Vyas, A., Gouripeddi, B., Zhang, Q., Wang, J., Komaragiri, V., Ragan, E., et al.: Captaincook4d: A dataset for understanding errors in procedural activities. *Advances in Neural Information Processing Systems* **37**, 135626–135679 (2024)
37. Qin, T., Li, P., Vins-mono, S.S.: A robust and versatile monocular visual-inertial state estimator., 2018, 34. DOI: <https://doi.org/10.1109/TRO> pp. 1004–1020 (2018)
38. Radford, A., Kim, J.W., Hallacy, C., Ramesh, A., Goh, G., Agarwal, S., Sastry, G., Askell, A., Mishkin, P., Clark, J., et al.: Learning transferable visual models from natural language supervision. In: International conference on machine learning. pp. 8748–8763. PmLR (2021)
39. Routray, S., Pan, H., Jain, U., Bahl, S., Pathak, D.: Vipra: Video prediction for robot actions. arXiv preprint arXiv:2511.07732 (2025)
40. Schönberger, J.L., Frahm, J.M.: Structure-from-motion revisited. In: Conference on Computer Vision and Pattern Recognition (CVPR) (2016)
41. Teed, Z., Deng, J.: Raft: Recurrent all-pairs field transforms for optical flow. In: European conference on computer vision. pp. 402–419. Springer (2020)
42. Tongyi Lab, Alibaba Cloud: Qwen3-vl-4b-instruct: Instruction-tuned vision-language model (2025), <https://huggingface.co/Qwen/Qwen3-VL-4B-Instruct>, model version: qwen3-vl-4b-instruct. Accessed: 2025-11-14
43. Tongyi Lab, Alibaba Cloud: Qwen3-vl: Advancing vision-language understanding with scalable multimodal pretraining (2025), <https://github.com/QwenLM/Qwen3>, accessed: 2025-11-14
44. Touvron, H., Lavril, T., Izacard, G., Martinet, X., Lachaux, M.A., Lacroix, T., Rozière, B., Goyal, N., Hambro, E., Azhar, F., et al.: Llama: Open and efficient foundation language models. arXiv preprint arXiv:2302.13971 (2023)
45. Wang, J., Zhang, Q., Chao, Y.W., Wen, B., Guo, X., Xiang, Y.: Ho-cap: A capture system and dataset for 3d reconstruction and pose tracking of hand-object interaction. arXiv preprint arXiv:2406.06843 (2024)
46. Wang, M., Xing, J., Liu, Y.: Actionclip: A new paradigm for video action recognition. arXiv preprint arXiv:2109.08472 (2021)

47. Wang, Q., Ye, V., Gao, H., Zeng, W., Austin, J., Li, Z., Kanazawa, A.: Shape of motion: 4d reconstruction from a single video. In: Proceedings of the IEEE/CVF International Conference on Computer Vision. pp. 9660–9672 (2025)
48. Wang, X., Zhao, K., Liu, F., Wang, J., Zhao, G., Bao, X., Zhu, Z., Zhang, Y., Wang, X.: Egovid-5m: A large-scale video-action dataset for egocentric video generation. arXiv preprint arXiv:2411.08380 (2024)
49. Wang, X., Kwon, T., Rad, M., Pan, B., Chakraborty, I., Andrist, S., Bohus, D., Feniello, A., Tekin, B., Frujeri, F.V., et al.: Holoassist: an egocentric human interaction dataset for interactive ai assistants in the real world. In: Proceedings of the IEEE/CVF International Conference on Computer Vision. pp. 20270–20281 (2023)
50. Wen, B., Trepte, M., Aribido, J., Kautz, J., Gallo, O., Birchfield, S.: Foundation-stereo: Zero-shot stereo matching. In: Proceedings of the IEEE/CVF conference on computer vision and pattern recognition. pp. 5249–5260 (2025)
51. Wen, J., Zhu, M., Zhu, Y., Tang, Z., Li, J., Zhou, Z., Li, C., Liu, X., Peng, Y., Shen, C., et al.: Diffusion-vla: Generalizable and interpretable robot foundation model via self-generated reasoning. arXiv preprint arXiv:2412.03293 (2024)
52. Xing, J., Xia, M., Zhang, Y., Chen, H., Yu, W., Liu, H., Liu, G., Wang, X., Shan, Y., Wong, T.T.: Dynamicrafter: Animating open-domain images with video diffusion priors. In: European Conference on Computer Vision. pp. 399–417. Springer (2024)
53. Xu, H., Ghosh, G., Huang, P.Y., Okhonko, D., Aghajanyan, A., Metze, F., Zettlemoyer, L., Feichtenhofer, C.: Videoclip: Contrastive pre-training for zero-shot video-text understanding. arXiv preprint arXiv:2109.14084 (2021)
54. Xu, M., Zhang, H., Hou, Y., Xu, Z., Fan, L., Veloso, M., Song, S.: Dexumi: Using human hand as the universal manipulation interface for dexterous manipulation. arXiv preprint arXiv:2505.21864 (2025)
55. Yang, A., Li, A., Yang, B., Zhang, B., Hui, B., Zheng, B., Yu, B., Gao, C., Huang, C., Lv, C., et al.: Qwen3 technical report. arXiv preprint arXiv:2505.09388 (2025)
56. Zhou, Z., Zhu, Y., Wen, J., Shen, C., Xu, Y.: Vision-language-action model with open-world embodied reasoning from pretrained knowledge. arXiv preprint arXiv:2505.21906 (2025)
57. Zhu, X., Liu, Y., Li, H., Chen, J.: Learning generalizable robot policy with human demonstration video as a prompt. arXiv preprint arXiv:2505.20795 (2025)
58. Zhu, Y., Feng, F.: Let me show you: Learning by retrieving from egocentric video for robotic manipulation. arXiv preprint arXiv:2511.05199 (2025)
59. Zitkovich, B., Yu, T., Xu, S., Xu, P., Xiao, T., Xia, F., Wu, J., Wohlhart, P., Welker, S., Wahid, A., et al.: Rt-2: Vision-language-action models transfer web knowledge to robotic control. In: Conference on Robot Learning. pp. 2165–2183. PMLR (2023)